Inorganic Chemistry

Article

pubs.acs.org/IC

The Peculiar Role of the Au_3 Unit in Au_m Clusters: σ-Aromaticity of the Au_5Zn^+ Ion

Yanle Li,[†,§] Vytor Oliveira,[‡,§] Chunmei Tang,[†] Dieter Cremer,*[,‡] Chunyan Liu,[†] and Jing Ma*[,†]

[†]Key Laboratory of Mesoscopic Chemistry of MOE, School of Chemistry and Chemical Engineering, Nanjing University, 22 Hankou Road, Nanjing, Jiangsu Province 210093, People's Republic of China

[‡]Computational and Theoretical Chemistry Group, Department of Chemistry, Southern Methodist University, 3215 Daniel Avenue, Dallas, Texas 75275-0314, United States

Supporting Information

ABSTRACT: The stability of small Au_m (m = 4−7) clusters is investigated by analyzing their energetic, geometric, vibrational, magnetic, and electron density properties. Gold clusters can be constructed from stable cyclic 3-center-2-electron (3c-2e) Au_3^+ units (3-rings) with σ-aromaticity. The stabilization requires a flow of negative charge from internal 3-rings with electron-deficient bonding to peripheral 3-ring units with stronger Au−Au bonds. The valence-isoelectronic clusters Au_6 and Au_5Zn^+ have similar electronic properties: Au_5Zn^+ is a strongly σ-aromatic molecule. An understanding of the structure of Au_m clusters is obtained by deriving a *Clar's Rule equivalent for polycyclic gold clusters*: The structure with the larger number of rings with dominant 3c-2e character and a smaller degree of 3c-3e character occupies the global minimum of the Au_m potential energy surface.

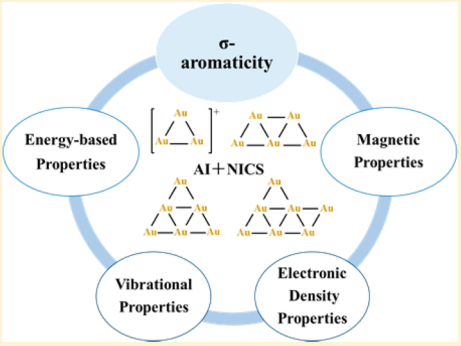

1. INTRODUCTION

Gold clusters have received enhanced interest in nanoscience because of their unique catalytic, electronic, and optical properties.[1−6] The pronounced scalar relativistic effects of gold lead to the fact that Au_m clusters exhibit unique structural and bonding properties that distinguish them from other metal clusters.[7−12] During the past three decades, pure gold clusters Au_m in the small-to-medium size range have been described in experimental and theoretical studies.

In 2008, Gruene and co-workers determined the structure of neutral Au_7, Au_{19}, and Au_{20} by comparing their experimental spectra obtained by far-IR multiple-photon dissociation (FIR-MPD) spectroscopy in the gas phase with the calculated vibrational spectra for multiple isomers.[7] De and co-workers investigated the finite temperature behavior of neutral Au_m (m = 3−10) clusters in the gas phase using molecular dynamical simulations based on relativistic density functional theory (DFT).[8] Zanti and Peeters studied Au_m ($m \leq 16$) clusters with B3LYP and explained their stability in terms of a donor−acceptor model, which suggested a cyclic flow of electrons within a cluster.[9] Sergeeva and Boldyrev demonstrated that small three-dimensional Au clusters could be built from the Au_4 tetrahedron characterized by 4c-2e bonding.[10] All these investigations established a deeper insight into the structure and thermodynamic stability of gold clusters. Recently, Xu and co-workers used the triangular, two-electron (2e) Au_3 (in short: $Au_3(2e)$) and rhombic $Au_4(2e)$ rings as elementary units to investigate the stabilities of 71 reported thiolate-protected Au nanoclusters developing and applying the Grand Unified Model (GUM).[11] On the basis of GUM, the authors not only rationalized the stabilities of known thiolate-protected gold nanoclusters but also predicted new ligand-protected gold nanoclusters of distinct stability. Gilb and co-workers studied small Au cluster cations (Au_m^+, m < 14) utilizing ion mobility measurements and computatinal methods and found that gold cluster cations had planar structures for m = 3−7 at room temperature.[12]

The concept of σ-aromaticity (stabilization by $4p$ + 2 σ-electrons in radial or $4p$ σ-electrons in tangential occupied orbitals, p = 0, 1, 2, ..., thus leading to aromatic Hückel and/or aromatic Möbius systems) can be traced to two different delocalization modes:[13,14] (i) *Peripheral (one-dimensional) delocalization along the σ-bonds*: In 1979, Dewar[15] discussed the small ring strain of cyclopropane and related this to the peripheral delocalization of σ-electrons. (ii) *Surface (two-dimensional) delocalization in the ring plane*: Cremer and Kraka[13,14] showed that σ-delocalization could lead to delocalization in the ring plane of cyclopropane, which in substituted cyclopropanes determined both geometry and stability. Later, Cremer and Gauss[16] provided further evidence for the phenomenon of surface delocalization. The potential σ-aromaticity of various small rings has caught the interest of many researchers.[17−19] The physical and chemical properties of hydrogen clusters,[20] polycyclophosphanes,[21] Zn_3^+ and Ge_4^{2+} clusters,[22,23] lanthanum-doped boron clusters,[24] and unsaturated cyclopropametallapentalenes[25,26] have also been rationalized in terms of σ-aromaticity or surface delocalization.

Received: February 14, 2017
Published: April 27, 2017

DOI: 10.1021/acs.inorgchem.7b00404
Inorg. Chem. 2017, 56, 5793−5803

Scheme 1. Structures[a] of Neutral Au_m Clusters, Au_3^+, $Au_2Zn^{1/2+}$, and Au_5Zn^+

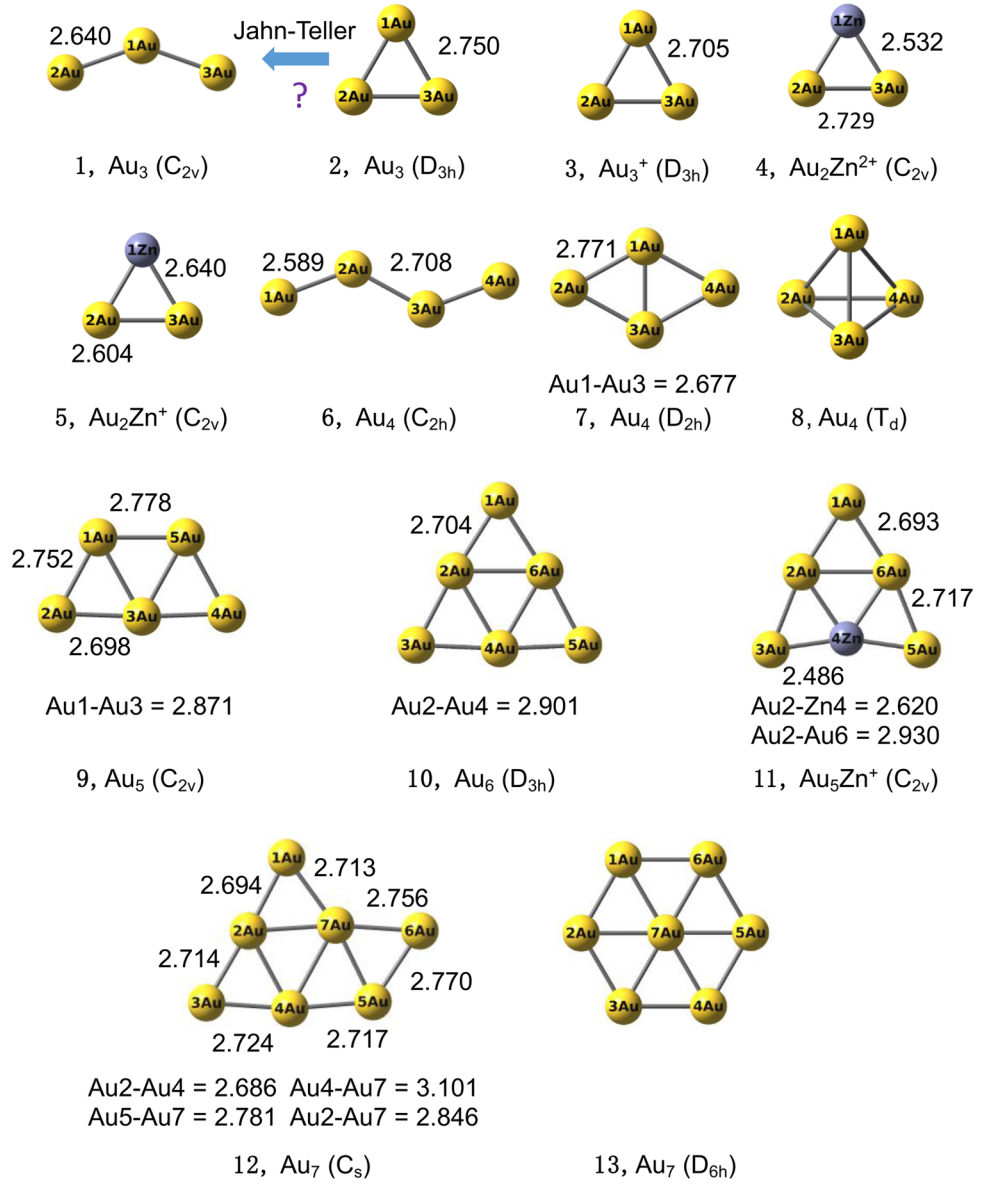

[a]The bond lengths (in Å) are given at the B3LYP/LANL2DZ level of theory.

To our knowledge, a systematic theoretical investigation of the stabilities of planar Au_m (m = 4−7) clusters as an aggregation of Au_3(2e) or Au_3(3e) building blocks has not been performed so far. As becomes obvious from Scheme 1, the ground states of Au_m clusters contain Au_3 units (Au_3 rings with $2 \leq p \leq 3$ electrons), suggesting a simple structural principle for gold clusters. In this work, we will present an electronic structure description of the Au_3 units based on their energetic, geometric, vibrational, magnetic, and electron density properties and use the outcome of this analysis to discuss structure and stabilities of planar Au_m clusters up to m = 7 for the purpose of obtaining a general building principle for Au_m clusters. Apart from this, Au_5Zn^+ will be analyzed, as it is an electronically interesting analogue of the Au_6 cluster and also a potential σ-aromatic cluster.[27]

2. COMPUTATIONAL DETAILS

Geometry optimizations and vibrational frequency calculations were performed for all Au_m clusters shown in Scheme 1 utilizing DFT. Becke's three-parameter hybrid exchange-correlation functional (B3LYP)[28,29] was used in connection with the LANL2DZ basis set[30−32] (for Zn, the 6-31G(d) basis set was employed). Preliminary calculations were also performed with the CAM-B3LYP,[33] M06,[34] M06-2X,[34] LC-ωPBE,[35−37] and ωB97XD[38] functionals. It turned out that B3LYP was more robust for the calculation of second-order response properties, and therefore most of the results were discussed for this hybrid functional. Each stationary point was verified to be a minimum on the potential energy surface with the help of the eigenvalues of the Hessian matrix of second derivatives. At the B3LYP/LANL2DZ level, the T_d-symmetrical Au_4 and the D_{6h}-symmentrical Au_6 clusters were located as stationary points with three and one imaginary frequencies, respectively, which was the reason why these two structures were not investigated in detail, although their relative stability was discussed in this work.

CCSD(T)[39] and PBEPBE-D3(BJ)[40−42] calculations with an aug-cc-pVTZ-PP basis set[43,44] were also performed to predict the atomization

DOI: 10.1021/acs.inorgchem.7b00404
Inorg. Chem. 2017, 56, 5793−5803

Scheme 2. Overview of the Methods Used in This Work[a]

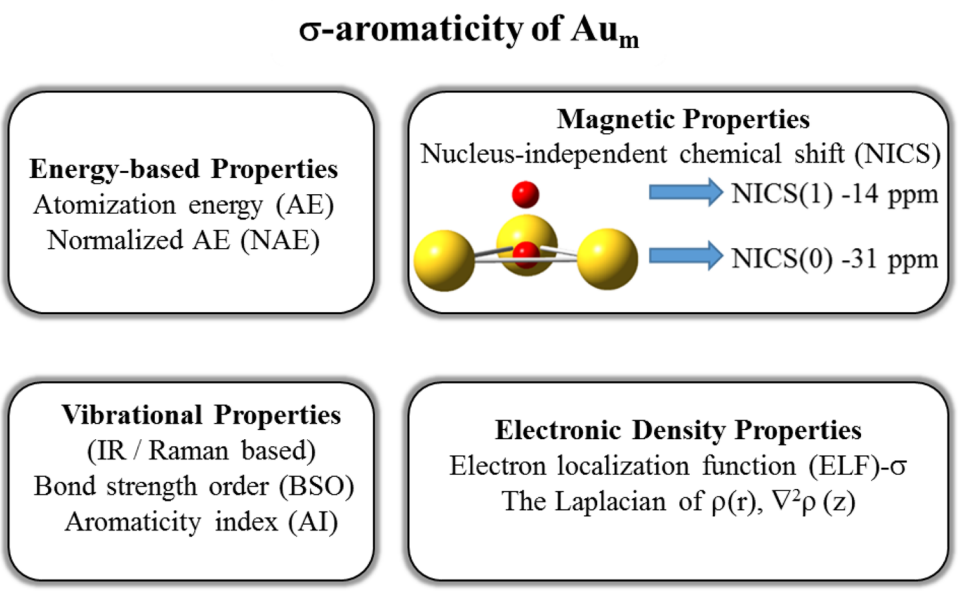

[a]The NICS(0) and NICS(1) values (in ppm) of Au_3^+ are taken at pre-chosen positions indicated by the red dots: for NICS(0), the geometrical center (centroid) of the ring is taken, for NICS(1) the position 1 Å above the centroid of the Au_3^+ ring.

energies (AE) and normalized AE (NAE or cohesive energy) of the planar clusters: NAE = AE/N, where N is the number of atoms in a molecule. In the case of the Au_3(3e) multireference system, CASSCF and broken-symmetry unrestricted DFT (BS-UDFT) calculations were performed to estimate its stability.

For the description of delocalization and potential aromaticity, we calculated the nucleus-independent chemical shift (NICS) parameters utilizing the Gauge-Independent Atomic Orbital (GIAO) method.[45−49] The NICS value gives the negative of the magnetic shielding computed at a prechosen position of the molecular geometry. In this work, NICS values are calculated at the centroids of the rings (denoted as NICS(0)) and 1.0 Å above the ring centroids (NICS(1)) to exclude to some extend the influence of the core electrons of Au (the atomic radius of Au is 1.35 Å) and to get a better description of σ-delocalization. Scheme 2 illustrates the NICS(0) and NICS(1) positions and their values for Au_3^+. The negative NICS(1) value means the existence of induced diatropic ring currents typical of an "aromatic" electron system, while a positive value suggests paratropic ring currents typical of an "antiaromatic" electron system.[50]

As a third aromaticity index, the electron localization function (ELF)-σ was determined.[51] ELF-σ is calculated at the bifurcation point of two ELF domains, which are dominated by the contributions of the σ orbitals. It reveals the degree of interaction between adjacent ELF domains: A larger ELF-σ value suggests that the electrons more strongly delocalize between adjacent domains. Because NICS and ELF-σ parameters are largely independent of method and basis set, we exclusively report here the B3LYP/LANL2DZ results.

To determine the intrinsic strength of an Au−Au bond, the vibrational modes of the Au_m clusters were analyzed. For this purpose, the $3N - 6$ normal vibrational modes (N: number of atoms) of a cluster were converted into local vibrational modes using the Konkoli−Cremer method.[52−54] Then the local bond stretching force constants k^a were calculated, as these provided a quantitative and reliable measure of the intrinsic bond strength.[55] Accordingly, k^a values could be used to determine a bond strength order (BSO). For this purpose, we used as suitable references the Au_2 dimer and the 3-ring Au_3^+ with its 3c-2e bonding. The two molecules have Au−Au bond orders of 1.000 and 0.333 according to simple molecular orbital (MO) theory. This is a possible choice to convert local Au−Au stretching force constants into BSO values n with the help of the power relationship

$$n = a(k^a)^b \quad (1)$$

where the constants a and b are determined via the two reference molecules and the requirement that for $k^a = 0$ the BSO value must be also zero.[56] Analysis of the relativistically corrected electron density obtained with the Dirac-exact Normalized Elimination of the Small Component (NESC) method[57,58] reveals that the MO-based assumption of bond orders given above underestimates bonding for Au_3^+. The more reliable Mayer bond orders[59,60] suggest n-values of 1.105 and 0.610 for Au_2 and Au_3^+, respectively (for B3LYP/LANL2DZ, k^a values of 1.567 and 0.833 mdyn/Å were obtained), which lead to a power relationship (1) with $a = 0.724$ and $b = 0.941$. All BSO values were calculated using eq 1 based on these constants.

Sometimes it is useful to scale BSO values so that the total number of valence electrons is reproduced. Although the scaled BSO values are no longer comparable with those of other molecules with different atoms, they provide an impression on the number of electrons in a 3-ring.

The charge distribution in the Au_m clusters was determined using the natural population analysis (NPA) by Weinhold and co-workers.[61] This approach was also employed to determine natural bond orders (NBOs) and to probe the possible existence of non-Lewis bonds with 3c-character.[61] The electron density analysis of Bader[62] was applied to find bond critical points (BCPs) and ring critical points (RCPs) of the electron density distribution $\rho(\mathbf{r})$. The Laplacian of $\rho(\mathbf{r})$ in the z-direction (normal to the ring plane), $\nabla^2\rho(z)$, was used to investigate any density concentration in the center of the 3-ring. Larger density concentration is indicated by a more negative $\nabla^2\rho(z)$ value.[62]

Cremer and co-workers have derived an aromaticity index (AI) from local stretching force constants and their associated BSO values n.[63,64] In this work, we extend the definition of AI to describe σ-delocalization and the nonclassical bonding character in Au_m clusters: For this purpose we use eq 2

$$\mathrm{AI} = 1 - \frac{\gamma}{N\mathrm{bonds}} \sum (n_{\mathrm{opt}} - n_i)^2 \quad (2)$$

where $n_{\mathrm{opt}} = 0.610$ gives the optimal BSO of Au_3^+ at the B3LYP/LANL2DZ level of theory, n_i the BSO value of the ith bond, Nbonds is the number of bonds in an Au_m ring, and $\gamma = 4.078$ is an adjustable parameter that sets the AI of the reference molecule Au_3^+ equal to 1 (or 100%) thus identifying a completely delocalized 3c-2e system. Any

DOI: 10.1021/acs.inorgchem.7b00404
Inorg. Chem. 2017, 56, 5793−5803

AI value smaller than 1 indicates a less delocalized σ-electron system. For AI = 0, classical covalent 2c-2e bonding is fully established as it is found in Au_2.

Parameters such as AI can be used to determine σ-aromaticity (peripheral delocalization in a Au_m ring), whereas $\nabla^2\rho(z)$ measures the concentration of the energy density at the RCP, which reflects the degree of surface delocalization and is especially important in organic 3-rings and π-complexes.[17,65] One can weight ρ(RCP) with $\nabla^2\rho(z)$ to get $\eta = |\rho(RCP)/\nabla^2\rho(z)|$, an area reflecting the extent of surface delocalization. If the concentration is large, the area becomes small as there is less delocalization; that is, concentration and delocalization of electrons are opposing properties. AI, $\nabla^2\rho(z)$, and η reflect the degree of electron delocalization, but they do not reflect other electronic factors such as ring strain or π-complex character of a 3-ring.[17] Therefore, the deviation d_i of the maximum electron density path (bond path) from the internuclear connection line at the BCP was calculated. Also, the extent of ring strain was evaluated by determining the deformation coordinates[66] R (breathing radius R of 3-ring; $R - R_0 = t_0$ is the deviation from a suitable reference radius R_0), t_1 (deformation amplitude), and ϕ_1 (deformation phase angle). Once the deformation coordinates are known, the associated local deformation force constants[66] can be calculated that provide a direct measure of ring strain. Calculations were performed with Gaussian09,[67] Molpro,[68] and the COLOGNE2016 program.[69] ELF calculations were performed with the Multiwfn package.[70]

3. RESULTS AND DISCUSSIONS

The optimized planar structures of Au_3^+, Au_m (m = 4−7), and cation Au_5Zn^+ are displayed in Scheme 1 (for the Cartesian coordinates of the equilibrium geometries, see the Supporting Information). All structures calculated are planar or nearly planar. Their relative stabilities are determined via the corresponding AE and NAE values (Table 1 and Figure S1).

Table 1 and Figure S1 reveal that Au_3^+ represents (compared with Au_6, Au_2Zn^{2+}, and Au_5Zn^+) a stable Au_m cluster (NAE, PBEPBE-D3(BJ): 47.3 kcal/mol; CCSD(T): 42.5 kcal/mol) comparable in its stability with Au_6 (46.1; 43.1 kcal/mol) and Au_7 (45.3 kcal/mol, Table 1). Noteworthy is that all Au clusters investigated have a larger NAE than Au_2 (27.3; 24.7 kcal/mol), which suggests that planar Au_m rings gain a significant amount of stabilization, which obviously has to do with electron delocalization in the 3-ring units.

Table 1. Calculated Atomization Energies (AE) and Normalized AE (NAE)[a]

	B3LYP/LANL2DZ[a]		PBEPBE-D3(BJ)/aug-VTZ-PP[a]		CCSD(T)[b]/aug-VTZ-PP	
	AE	NAE	AE	NAE	AE	NAE
$Au_2(D_{\infty h})\rightarrow$ 2Au (^{2}S)	43.2	21.6	54.6	27.3	49.5	24.7
$Au_3^+(2e)(D_{3h})\rightarrow$2Au (^{2}S) + 1Au$^+$(^{1}S)	113.2	37.7	142.0	47.3	127.6	42.5
$Au_3(3e)$ $(D_{3h})\rightarrow$3Au (^{2}S)	58.3	19.4	83.6	27.9	73.3	24.4
$Au_3(3e)$ $(C_{2v})\rightarrow$3Au (^{2}S)[c]	63.5	21.2	86.7	28.9	72.5	24.2
Au_4 (D_{2h}) →4Au (^{2}S)	107.5	26.9	147.1	36.8	134.6	33.6
Au_4 (C_{2h}) →4Au (^{2}S)	102.0	25.5	136.7	34.2	118.2	29.5
$Au_5(C_{2v})$ →5Au (^{2}S)	147.7	29.5	202.1	40.4	184.6	36.9
$Au_6(D_{3h})\rightarrow$6Au (^{2}S)	208.1	34.7	276.5	46.1	258.6	43.1
$Au_7(C_s)\rightarrow$7Au (^{2}S)	232.6	33.2	317.3	45.3	278.9	39.8
$Au_2Zn^+(C_{2v})$ →2Au (^{2}S) + Zn$^+$(^{2}S)	97.8	32.6	110.7	36.9	79.7	26.6
$Au_2Zn^{2+}(C_{2v})$ →2Au (^{2}S) + Zn^{2+}(^{1}S)	216.6	72.2	238.6	79.5	216.1	72.0
$Au_5Zn^+(C_{2v})$ →5Au (^{2}S) + Zn$^+$(^{2}S)	271.2	45.2	317.7	52.9	296.2	49.4

[a]In kilocalories per mole. [b]CCSD(T) energies at PBEPBE-D3(BJ)/aug-cc-pVTZ-PP geometries. [c]Broken symmetry solutions. UPBEPBE leads to one imaginary frequency of 210 i cm^{-1}.

The energy differences between the frontier orbitals of Au_3^+, Au_m, and Au_5Zn^+ calculated with different exchange-correlation (XC) functionals are shown in Figure 1 and Table S1. Although

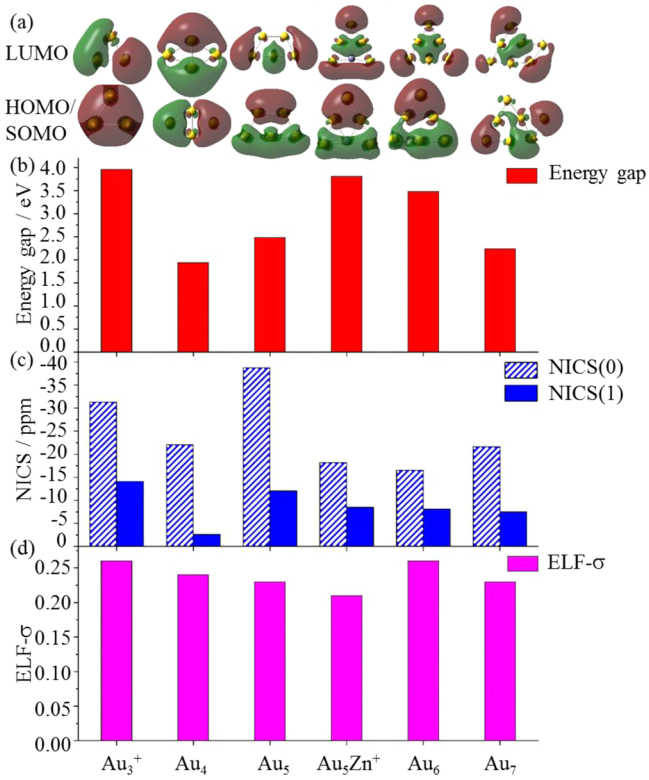

Figure 1. Comparison of some properties of Au_3^+, Au_m (m = 4−7), and Au_5Zn^+. (a) Perspective drawings of the HOMO, singly occupied molecular orbital (SOMO), or LUMO. All MO drawings are obtained at the RHF (ROHF) level of theory. (b) Bar diagram of the corresponding energy gaps $\Delta\varepsilon$. (c) Bar diagram of NICS(0) and NICS(1) values given for Au_m. (d) Bar diagram of ELF-σ values given for Au_m. B3LYP/LANL2DZ calculations.

the magnitude of the highest occupied molecular orbital−lowest unoccupied molecular orbital (HOMO−LUMO) energy gaps, $\Delta\varepsilon$, changes with the XC functional used, all XC functionals (with the exception of PBEPBE) predict the same order of $\Delta\varepsilon$ values: $Au_3^+ > Au_5Zn^+ > Au_6 > Au_5 > Au_7 > Au_4$. This trend does not exactly follow the trend of the calculated NAE in Table 1, but there are some similarities.

In addition to the energy gaps, the results of the NICS and ELF-σ calculations are shown in Figure 1 and Table S1. The difference in the NICS(0) and NICS(1) values indicates that the σ frame has significant influence on NICS(0), which makes it advisible to base the analysis of the magnetic properties of the Au clusters investigated exclusively on NICS(1).

The NBO analysis of Au_3^+ confirms that the 6s orbitals of the Au atoms form an a_1'-symmetrical, bonding 3c-orbital, that is, a fully delocalized orbital. Hence, it is justified to speak of a σ-aromatic 2e-ensemble that determines the stability and geometry of Au_3^+. The scalar relativistic contraction of the 6s(Au) orbital and the positive charge both lead to a decrease of the energy of the 3c orbital, a shortening of the Au−Au

DOI: 10.1021/acs.inorgchem.7b00404
Inorg. Chem. 2017, 56, 5793−5803

bonds, thereby an increase of the Au−Au bond strength, and an overall stabilization of the cation. Kalescky and co-workers[71] have coined in this connection the term electronegativity-driven increase of bond strength, which applies in the case of Au_3^+ as the effective electronegativity of Au increases with regard to the 6s electrons. Scalar relativity also leads to an expansion of the 5d lone pair orbitals and to an increase of their energies, which leads to overall destabilizing contributions. The strong decrease of the a_1' HOMO relative to the e′ LUMOs causes the increase in $\Delta\varepsilon$ (Figure 1, Table S1). This observation causes two questions, which must be answered in the following: (i) Is σ-electron delocalization a typical phenomenon for Au clusters? (ii) The 3e system Au_3 in its $^2E'$ state does undergo a Jahn−Teller distortion from D_{3h} to C_{2v},[72] which leads to a bent $Au_3(^2A')$ structure. The question is whether σ-electron delocalization is also observed in this case.

Investigation of acyclic Au_3 ($^2A'$) leads to a BSO value of 0.746 that suggests a 3e delocalization of the Au 6s electrons and a concomitant increase in the intrinsic bond strength from 0.610 (Au_3^+) to 0.746 (reduction of the Au−Au bond lengths from 2.705 to 2.640 Å). At this point a caveat is needed regarding the Jahn−Teller unstable D_{3h}-symmetrical Au_3(3e). Guo and co-workers[6] have performed for Au_3(3e) and its excited states multireference relativistic configuration interaction (CI) calculations, which explicitly include the effects of spin−orbit coupling (SOC). Their results reveal that (i) the Jahn−Teller distortion is relatively small and that (ii) SOC quenches the Jahn−Teller distortion so that the D_{3h} structure becomes more stable than the C_{2v} structure. Laser experiments confirm a D_{3h} symmetrical ground state.[6]

DFT in combination with an effective core potential such as LANL describes SOC only implicitly and in an averaged way so that its effect can be underestimated. At the BS-UB3LYP/LANL2DZ level of theory, the D_{3h} symmetrical form is a minimum (Table 1). Nevertheless, the acyclic Au_3 ($^2A'$) form is somewhat more stable than the cyclic Au_3(3e) form, but both are much less stable than Au_3^+ (PBEPBE, NAE: 28.9 and 27.9 vs 47.3 kcal/mol, Table 1). Strong SOC effects are only observed for open-shell systems with a fractional occupation of p, d, and f orbitals, whereas for closed-shell systems or open-shell systems with singly occupied s-orbitals, SOC effects are relatively small. Hence, the discussion of the electronic structure of the latter is reasonable.

SOC plays a role when comparing the D_{2h}-symmetrical Au_4 gold cluster with the acyclic C_{2h}-symmetrical Au_4. The latter might be viewed as two Au_2 units interacting via weak noncovalent interactions. σ-Delocalization changes this picture dramatically by establishing a relatively strong Au2−Au3 bond (BSO: 0.545; bond Au1−Au2: 1.028, Table 2). D_{2h}-Symmetrical Au_4 is more stable than C_{2h}-symmetrical Au_4 by 5.5 kcal/mol (or 1.4 kcal/mol per Au atom). Apart from these considerations, it is safe to say on the basis of the data shown in Tables 2, 3, and 4 that in acyclic and cyclic Au_m systems, there is a pronounced tendency for σ-electron delocalization that strongly influences the stability of the various clusters. Our results suggest that the formation of multiple σ-aromatic 2e Au_3^+ units (or distorted Au_3(3e) units) within a polycyclic Au_m cluster lead to extra stability as will be discussed in the following in more detail.

Each of the gold clusters investigated is formed by 3-ring units (denoted as **a**, **b**, **c**, **d**, **e** from the core of an Au_m cluster to its periphery and in line with its symmetry properties; Figure 2). The NICS(1) values for each of the 3-ring units are listed in Table 3. They reveal that NICS(1) values decrease with increasing annelation and decreasing positive charge of an Au_3 ring. For the Au_3 units in Au_3^+, Au_5, and Au_6 (in total five different Au_3 rings in different clusters, called **a**@ Au_5, etc.) an exponential decay of NICS(1) with the parameter of the number of shared edges in a polycyclic structure (n_{share}) can be observed suggesting a decrease of aromatic σ-delocalization for the inner rings (Figure 3).

Free Au_3^+ possesses the most negative NICS(1) value (−14.1 ppm) in line with its positive charge and the optimal 2e-delocalization. In Au_5, the central ring **a** shares one edge with each adjacent Au_3 unit. In this case, the NICS(1) value of ring **b** is reduced to −11 ppm, whereas that of ring **a** is lowered to −9 ppm. Defining the number of the shared edges by the parameter n_{share}, the NICS(1) values vary from −9 ppm (n_{share}: 2) to −8 ppm (n_{share}: 3). This trend is qualitatively maintained for Au_7 (Table 3) and reminds of the tendency of π-aromatic polybenzoides to prefer the structure with the largest number of aromatic sextets according to the Clar's rule.[63,73] The Clar's rule has also been used for inorganic BN analogues of polybenzenoid hydrocarbon systems.[74]

In this sense, the value of n_{share} might be used to explain the relative low stability of isomers of the nonplanar Au_4 and Au_7 clusters. For Au_4 (T_d), n_{share} has a value of 6 that is larger than

Table 2. Bond Distances r (Å), Local Force Constant k^a (mdyn/Å), and BSO Values n for the Gold Clusters Investigated

molecule (sym)	bond	r	k^a	BSO n
Au_3^+ (D_{3h})	Au−Au	2.705	0.833	0.610
Au_3 (D_{3h})	Au−Au	2.750	0.785	0.577
Au_3 (C_{2v})	Au1−Au2	2.640	1.032	0.746
Au_2Zn^+ (C_{2v})	Zn−Au	2.640	0.230	0.182
	Au−Au	2.604	1.439	1.020
Au_2Zn^{2+} (C_{2v})	Zn−Au	2.532	0.753	0.555
	Au−Au	2.729	0.821	0.602
Au_4 (D_{2h})	Au1−Au2	2.771	0.462	0.350
	Au1−Au3	2.677	0.958	0.696
Au_4 (C_{2h})	Au1−Au2	2.589	1.452	1.028
	Au2−Au3	2.708	0.740	0.545
Au_5 (C_{2v})	Au1−Au2	2.752	0.634	0.472
	Au1−Au3	2.871	0.285	0.223
	Au1−Au5	2.778	0.593	0.443
	Au2−Au3	2.698	0.846	0.619
Au_5Zn^+ (C_{2v})	Au1−Au2	2.693	0.934	0.679
	Au2−Au3	2.717	0.844	0.618
	Au2−Zn4	2.620	0.568	0.425
	Au2−Au6	2.930	0.345	0.266
	Au3−Zn4	2.486	1.040	0.751
Au_6 (D_{3h})	Au1−Au2	2.704	0.855	0.625
	Au2−Au4	2.901	0.339	0.262
Au_7 (C_s)	Au1−Au2	2.694	0.909	0.662
	Au1−Au7	2.713	0.806	0.591
	Au2−Au3	2.714	0.798	0.586
	Au2−Au4	2.686	0.373	0.287
	Au2−Au7	2.846	0.420	0.320
	Au3−Au4	2.724	0.766	0.564
	Au4−Au5	2.717	0.802	0.589
	Au4−Au7	3.101	0.087	0.073
	Au5−Au6	2.770	0.560	0.420
	Au5−Au7	2.781	0.519	0.391
	Au6−Au7	2.756	0.592	0.442

DOI: 10.1021/acs.inorgchem.7b00404
Inorg. Chem. 2017, 56, 5793−5803

Table 3. Results of NICS and the Electron Density Analysis

	a	b	c	d	e
		NICS(1)/NICS(0)[a]			
Au_3^+	−14.08				
Au_2Zn^{2+}	−37.71/−14.32				
Au_4	−2.48				
Au_5	−9.03	−11.48			
Au_5Zn^+	−9.96	−12.60	−11.93		
Au_6	−8.14	−11.41			
Au_7	−6.27	−7.68	−8.52	−10.59	−8.64
		electron density analysis[b]			
Au_3^+					
η	1.652				
$\nabla^2\rho(z)$	−0.023				
Au_4					
η	1.619				
$\nabla^2\rho(z)$	−0.021				
Au_5					
η	1.688	1.684			
$\nabla^2\rho(z)$	−0.016	−0.019			
Au_5Zn^+					
η	2.000	1.818	1.700		
$\nabla^2\rho(z)$	−0.009	−0.011	−0.020		
Au_6					
η	1.714	−1.684			
$\nabla^2\rho(z)$	−0.014	−0.019			
Au_7					
η	1.692	1.667	1.650	1.619	1.684
$\nabla^2\rho(z)$	−0.013	−0.015	−0.020	−0.021	−0.019

[a]In units of parts per million. [b]Given in form of the Laplacian at the RCP in z-direction, $\nabla^2\rho(z)$, and the relative electron density weighted by the Laplacian $\rho/\nabla^2\rho(z)$ for the gold clusters investigated. B3LYP calculations. The symbol $\eta = |\rho(RCP)/\nabla^2\rho(z)|$ gives an area reflecting the extent of surface delocalization (see text). The Laplacian of ρ is given in e/bohr^5, and η is in bohr^2.

Table 4. Aromaticity Index (AI), Deformation Coordinates (Å), and Local Deformation Force Constants (mdyn/Å)[a]

cluster	AI	electrons[b]	R or t_0	k^a (R)	$q(t_1)$	k^a (t_1)
Au_3^+						
a	1.000	2.000	1.561	8.880	0.000	3.477
Au_2Zn^{+c}						
a	0.274	3.000	0.018	6.951	0.014	4.596
Au_2Zn^{2+c}						
a	0.992	2.000	1.499	8.062	0.077	3.666
Au_4	0.725 (p)					
a	0.807	2.000	0.021	7.533	0.036	3.801
Au_5	0.946 (p)					
a	0.553	1.084	0.079	4.213	0.036	2.135
b	0.770	1.958	0.040	5.172	0.059	1.592
Au_6	0.999 (p)					
a	0.506	0.520	0.114	3.525	0.000	1.430
b	0.835	1.827	0.037	5.793	0.077	1.781
$Au_5Zn^{+c,d}$	0.891 (p)					
a	0.474	0.643	0.071	4.860	0.122	1.484
b	0.929	1.820	0.006	7.503	0.077	3.801
c	0.826	1.717	0.038	5.964	0.092	1.833
Au_7	0.959 (p)					
a	0.352	0.484	0.134	2.049	0.095	0.469
b	0.542	1.166	0.091	2.174	0.140	0.512
c	0.848	1.502	0.038	6.024	0.008	2.257
d	0.882	2.010	0.027	6.512	0.056	2.152
e	0.854	1.838	0.037	5.912	0.058	1.880

[a]B3LYP calculations. The symbol (p) denotes the AI value based on the peripheral bonds. [b]Number of electrons in a ring unit based on scaled BSO values. [c]Values for t_0 were obtained with the R value of Au_2Zn^{2+} as reference. [d]The AI values obtained with Au_2Zn^{2+} as reference are given in the text (see also Supporting Information).

n_{share} = 1 for Au_4 (D_{2h}) thus suggesting that the latter is more stable. The nonplanar Au_4 (T_d) cluster turns out to be a saddle point of first order at the B3LYP level of theory. Similarly, n_{share} is 6 for Au_7 (D_{6h}), whereas it is just 4 in Au_7 (C_s), again explaining the lower stability of the former that is also a saddle point rather than a minimum. In other cases, the n_{share} value can be used to predict qualitative trends (see Table 3: Au_7). It can be expected that the value of n_{share} increases when the size of planar Au_m clusters becomes larger, suggesting the decrease of σ-aromaticity or instability of the planar structures of Au_m. The energy difference between the planar and nonplanar structures will be decreased with the increasing of the cluster size, rationalizing the tendency that planar Au_m clusters are no longer stable for larger m. The investigation of larger planar clusters is currently performed in our laboratories.

In general, both NAE and NICS(1) provide a measure too crude to correctly predict the relative stability of the neutral and cationic Au clusters investigated. The same holds for the energy gap $\Delta\varepsilon$ and the ELF-σ values. The latter are almost the same for all clusters (Figure 1). Therefore, other properties of the clusters were investigated, which relate to their electron density distribution and vibrational modes.

Listed in Tables 2, 3, and 4 are the calculated bond distances r, local stretching force constants k^a, their associated BSO values n (Table 2), the properties of the electron density distribution at the RCP in the form of the Laplacian of $\rho(\mathbf{r})$ in z-direction (Table 3), as well as the deformation coordinates and the associated force constants (Table 4). These properties will be discussed for each system in detail, where however some general remarks are first appropriate. (i) The analysis of the bond paths of the electron density distribution revealed only minor deviations from the internuclear connection lines, and therefore T-shaped or star-shaped structures can be excluded. However, it is relevant how strong RCPs are shifted away from the geometrical center of a ring toward one of the bonds. This is shown in Figure S2 in the Supporting Information. (ii) There is little evidence for surface delocalization in the center of the ring. Table 3 reveals that the η values decrease only slightly from an inner Au_3 unit to an outer one; that is, the inner unit has a somewhat larger degree of surface delocalization, but η ($1.6 < \eta < 2$ bohr^2) is in general too small because of a too small $\rho(\mathbf{r})$.

Au_4 ($^1B_{1u}$, D_{2h}). The square form of Au_4 is Jahn−Teller unstable and can be stabilized either by rectangular or rhombic distortion.[66] The latter leads to a planar bicyclic form with two 3-rings in which the four 6s(Au) electrons avoid peripheral delocalization and Jahn−Teller destabilization as much as possible as documented by a peripheral AI of 0.725. D_{2h}-Symmetrical Au_4 is best described as a central Au_2 unit that donates some negative charge to the two apical Au atoms (see NPA values in Figure 2). To avoid the less stable 3c-3e bonding situation of the 3-ring the apical bond lengths are weakened (BSO: 0.350, Table 2), and σ-delocalization is suppressed. Note that the AI(**a**) value of 0.807 is misleading insofar as both 3-rings compete for the electrons of the central bond. If these are

DOI: 10.1021/acs.inorgchem.7b00404
Inorg. Chem. 2017, 56, 5793−5803

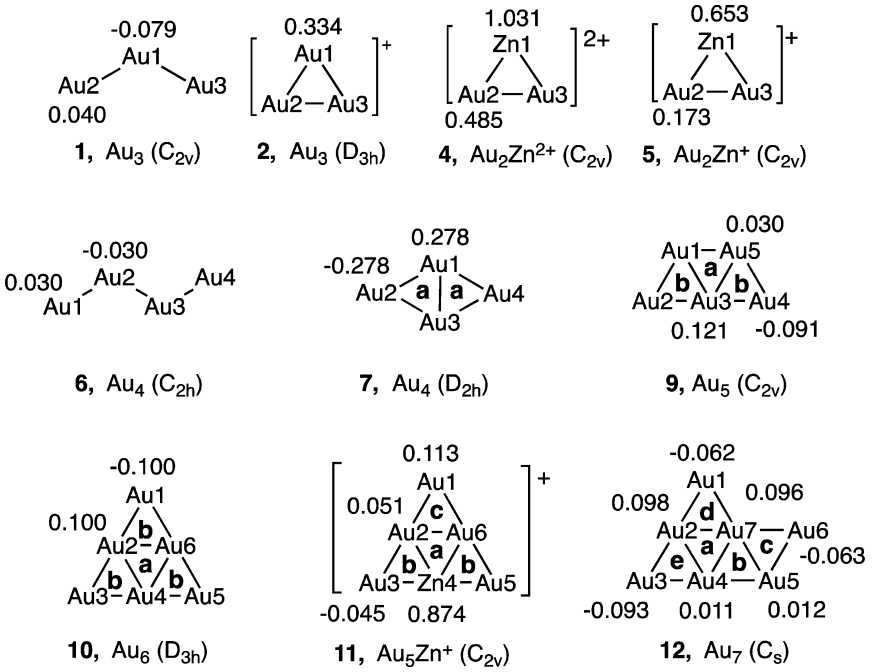

Figure 2. NPA charges for the clusters investigated, taken from B3LYP calculations. The 3-ring units are indicated by a letter code (**a**, **b**, **c**, etc).

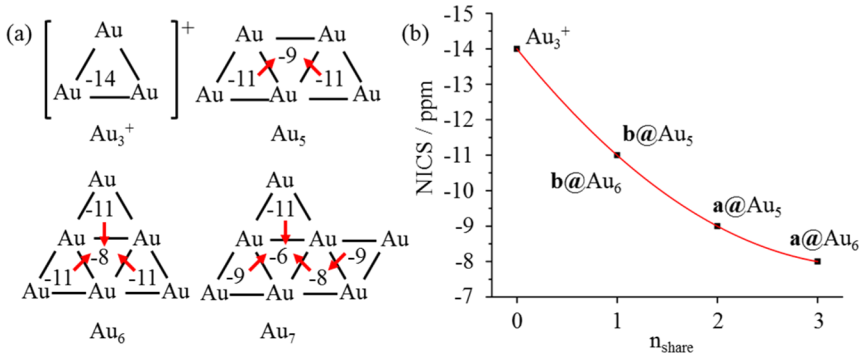

Figure 3. (a) The NICS(1) values of five Au_3 units. The red arrow points to less negative NICS(1) values. (b) The NICS(1) values of the Au_3 units in Au_3^+, Au_5, and Au_6 decrease in dependence of the parameter n_{share} that denotes the number of shared edges of a ring. The letters **a** and **b** indicate different 3-rings in Au_5 or Au_6 clusters (see Figure 2).

split up (by dividing the BSO value by 2), an AI value of just 0.722, like the peripheral delocalization of 0.725, is obtained.

Consequently, the absolute NICS(1) value of Au_4 is with |−2.5| ppm extremely low (Table 3). At the RCP (which is removed from the central bond; see Supporting Information) the degree of surface delocalization is small as indicated by a compact delocalization region (η = 1.619 bohr^2, smallest value for all 3-rings investigated, Table 3), which is typical of a slightly positively charged central bond attracting two apical negatively charged Au atoms. This is in line with a low NAE value of just 33.6 kcal/mol (CCSD(T), Table 1). Noteworthy is that the positive charge of the bridge atoms reduces their covalent radius so that the Au1−Au3 distance becomes shorter.

If one scales the BSO values so that they add up to the number of σ-type valence electrons of Au_m (note that this leads to a loss of the comparability of local force constants and BSO values between different metal clusters), one obtains 2e for the Au−Au bridge of Au_4 and 2e for the four bonds connecting the apical Au atoms to the bridge. The four apical bonds have only slight concave character (i.e., there is no π-complex character[54,55]), which confirms that bonding in the Au_m clusters is different from what is known from organic systems having the possibility of involving pπ-orbitals.

The analysis of the electronic structure of Au_4 reveals that the equilateral Au_3(3e) units in a polycyclic system prefer to distort. In T_d-symmetrical Au_4, symmetry and the polycyclic structure freeze the molecule in four unstable, equilateral 3c-3e units, which are prevented in the more stable rhombic D_{2h}-symmetrical form. Apart from this, the T_d-symmetrical Au_4 or the D_{6h}-symmetrical Au_7 cluster with its six destabilized 3c-3e units can only distort by ring breathing, that is, a concerted bond lengthening, and an overall weakening of the structure without effectively stabilizing the structure. This clarifies the chemical basis of the parameter n_{share}: polycyclic Au_m structures with high symmetry and a large n_{share} parameter enforce equilateral Au_3(3e) units and therefore cause instability.

In passing we note that the D_{2h}-symmetrical Au_4 cluster can be stabilized by opening one of the 3-rings and forming a more stable C_{2v}-symmetrical structure[9] for which it is easier to realize a 3c-2e unit.

Au_5 ($^2A'$, C_{2v}). The ground state is a doublet radical with five 6s electrons that is characterized by a peripheral AI of 0.946,

DOI: 10.1021/acs.inorgchem.7b00404
Inorg. Chem. 2017, 56, 5793−5803

whereas AI(**a**) = 0.553 and AI(**b**) = 0.770. Au_5 can be viewed as two overlapping Au_4 units with a common central ring **a**, so that Au1 and Au5 are both apex atom and bridge atoms at the same time (Figure 2), which leads to an effective atomic charge close to zero (0.030e; Figure 2). The bridge bonds Au1−Au3 and Au3−Au5 become labialized (BSO 0.223) because of a strong electron deficiency resulting from the fact that seven Au−Au bonds must be formed with just five electrons corresponding to 65% electron deficiency (9e of 14e are missing; Au_4: 6e of 10e, i.e., 60% deficiency). Scaled BSO values reveal that there is effectively just one electron in ring **a** and two electrons in each ring **b** (Table 4). Peripheral electron delocalization involving somewhat more than 4.2e is preferred.

Aromatic σ-delocalization is stronger in ring **b** (AI = 0.770) than in ring **a** (AI = 0.553, Table 4), in line with the Clar's rule for gold clusters (generation of largely independent 3c-2e units similar to the situation of 6c-6e π-units in phenanthrene[63]) and the NICS results. The surface delocalization values are comparable in **b** (1.684 bohr^2) and in **a** (1.688 bohr^2, Table 3). They are slightly larger than in the reference molecule Au_3^+ thus indicating a somewhat increased tendency of surface delocalization because of the symmetry and topology of the bonding network.

The stability of two largely independent 3c-2e units in Au_5 (topologically not possible in Au_4) is confirmed by the increased NAE value (CCSD(T): 36.9 kcal/mol as compared to just 33.6 kcal/mol in Au_4; Table 1). The extra stability of Au_5 can also be documented by the breathing force constants[66] $k^a(R)$, which for ring **b**@Au_5 are significantly larger than those at ring **a**@Au_5 but smaller compared to the corresponding Au_4 value (breathing force constant, **b**@Au_5: 5.172 mdyn/Å; Au_4: 7.533 mdyn/Å, Table 4). Ring **b**@Au_5 can easily be distorted to avoid the unstable 3c-3e situation (distortion amplitude t_1 = 0.059 Å, distortion force constant $k^a(t_1)$ = 1.592 mdyn/Å, Table 4), which is more difficult for **a**@Au_4 (t_1 = 0.036 Å; $k^a(t_1)$ = 3.801 mdyn/Å, Table 4), as the latter has only the possibility of moving the apex atoms away from the bridge Au1−Au3, which leads to dissociation.

Au_6 (^1A_g, D_{3h}). If another Au atom is added to Au_5 then the most stable structure of Au_6 is formed as a planar D_{3h}-symmetrical cluster with three largely independent 3c-2e units and a central ring **a** that has a positive charge of +0.3 e (NBO value) and long, weak bonds (2.901 Å, BSO: 0.262). Scaled BSO values suggest that just 0.520e (Table 4) are forming the central ring. Its AI is relatively low (0.506) as is its breathing constant of 3.525 mdyn/Å (Table 4).

Ring **b** has stronger bonds (BSO: 0.625) and contains (after scaling) 1.827e in line with the ideal 3c-2e situation. Accordingly, both its AI and $k^a(R)$ value are high: 0.835 and 5.793 mdyn/Å. The three rings **a** form a peripheral six-bond Au_6 triangle with the perfect AI value of 0.999 (Table 4). Since the stabilities of the peripheral Au_6 triangle and the three peripheral rings dominate the overall stability of the cluster, the NAE value of 43.1 kcal/mol is even somewhat larger than that of Au_3^+ (42.5 kcal/mol; Table 1).

Au_7 ($^2A'$, C_s). Adding another Au atom to Au_6 leads to Au_7, which in its most stable form has five different 3-rings. These can be viewed as being formed from a bicyclic Au_4 unit (rings **a** and **b**) with three peripheral 3c-2e-rings **c**, **d**, and **e**. The AI values (0.352 (**a**), 0.542 (**b**), 0.848 (**c**), 0.882 (**d**), 0.854 (**e**)) are similarly ordered as the $t_0 = R - R_0$ or $k^a(R)$ values: 0.134 (**a**), 0.091 (**b**), 0.038 (**c**), 0.027 (**d**), 0.037 Å (**e**) and 2.049 (**a**), 2.174 (**b**), 6.024 (**c**), 6.512 (**d**), 5.912 mdyn/Å (**e**). This suggests a decreased stability (increased breathing deformation) in the series **d** ≈ **e** > **c** ≫ **b** ≫ **a** in line with the 3c-2e Clar's rule for Au_m.

For all Au_m investigated, bridge Au atoms have positive NPA charges, whereas apex atoms have negative charges (Figure 2). This is also the case for rings **d** (−0.062), **e** (−0.093), and **c** (−0.063 e) in Au_7. Scaled BSO values suggest that ring **d** is closest to the ideal 3c-2e situation (2.010 e), followed by rings **e** (1.838), **c** (1.502), **b** (1.166), and **a** (0.484 e). These observations are in line with the 3c-2e Clar's rule, the NICS values, and an NAE value of 45.3 kcal/mol (compared to 46.1 kcal/mol for Au_6; PBEPBE-D3(BJ), Table 1), which results of course from the stability of three external relatively stable 3-rings.

Au_5Zn^+($^1A_1$, C_{2v}). This molecule has been previously described as a σ-aromatic system.[27] We have now the means to quantify this description by comparing with Au_2Zn^{2+} as a reference ion. The latter has an AI of 0.992; that is, it is also a σ-aromatic 3c-2e system. It is a suitable reference system to analyze Au_5Zn^+. For this purpose, eq 2 was reparametrized to obtain reasonable AI values (see Supporting Information). The three peripheral rings of Au_5Zn^+ have AI values of 0.929 (**b**) and 0.826 (**c**), whereas ring **a** has an AI of just 0.474. This again indicates a large degree of σ-delocalization because of the positive charge, which is distributed over the atoms of rings **a** and **c**: Au1 (0.113), Au2 (0.051), Zn4 (0.874e, Figure 2). The bonds involving Zn become stronger (BSO values of 0.751 and 0.425 vs 0.625 and 0.262 in Au_6, Table 2), which is because of the higher electronegativity of Zn (Pauling scale: 1.65 vs 1.42 for Au) especially in view of its high positive charge.

Theoretically, when splitting up charges always equally, the six valence electrons could be equally distributed among rings **c**, 2 × **b**, and **a**: 1.666; 1.666; 1.666; 1.000. The NPA charge distribution gives ratios of 1.519:1.737:1.737:1.007 thus suggesting that ring **c** loses charge that is drawn into the two rings **b** and to the more electronegative Zn atom (at Zn the charge is reduced from +1 to 0.874e) and Au3 as well as Au5 (−0.045e). The charge of ring **a** does not change much so that this ring is just a means for the charge flow from Au1 to the base.

Since the covalent bonding radius of Zn^+ is much smaller than that of Au or Au^+, the D_{3h}-symmetrical triangle of Au_6 becomes a C_{2v}-symmetrical structure with inwardly bent Au3−Zn4−Au5 unit (see bond path diagram in Supporting Information) so that Zn^+ is "inside" the ring structure and bonds are much stronger. Both the AI (Table 4) and NICS(1) values (Table 3) confirm strong σ-delocalization: **b** (−12.6) < **c** (−11.9) < **a** (−10.0 ppm, Table 3). Au_5Zn^+ is more stable than the valence isoelectronic Au_6 as is confirmed by a high NAE value of 49.4 kcal/mol (CCSD(T), Table 1).

The optimal form of Au_5Zn^+ must contain Zn in a central rather than apical position. Only in this way is the delocalization of some of the positive charge limited to rings **a** and **c** and leaves the apical atoms Au3 and Au5 negatively charged. The deformation force constants confirm the order of ring stabilities (Table 4) and, together with AI and NICS values, predict Au_5Zn^+ as an exceptionally stable σ-aromatic cation.

4. CONCLUSIONS

Gold clusters have a strong tendency to adopt structures built from 3-ring units. This is a direct result of the extra stability of the Au_3^+(2e) unit, which benefits from σ-electron delocalization

DOI: 10.1021/acs.inorgchem.7b00404
Inorg. Chem. 2017, 56, 5793−5803

partially caused by scalar relativistic effects. Adding another electron to obtain the neutral Au_3(3e) leads to a Jahn−Teller unstable system, which must distort to gain stability. This is most pronounced in polycyclic structures because of the difficulty of distorting a highly symmetric structure in an effective way. Examples are the T_d-symmetrical Au_4 or the D_{6h}-symmetrical Au_7 that are both stationary points of cluster rearrangements. The D_{2h}-symmetrical Au_4 can better distort, however, for the price of a relatively small peripheral AI value leading to a central Au_2 unit attracting two apical Au atoms.

AI, NICS, and deformation parameters suggest a simple building principle for small Au_m clusters that is closely connected to the relative stabilities of Au_3^+(2e) and Au_3(3e) systems. If a 3-ring can be converted into a unit adopting some features of the Au_3^+, stability will be achieved by σ-aromaticity. For the small Au_m clusters investigated, a distorted 3-ring is always possible if three-dimensional clusters are avoided. In the two-dimensional structures, the use of 3-rings as building blocks leads to a steep increase in the number of bonding interactions that require electron-deficient bonding. This in turn enforces electron sharing between 3-rings and a move of negative charge from the more central 3-rings to the peripheral 3-rings so that the latter can adopt 3c-2e units of larger stability with relatively strong bonding on the outside and weak (electron-deficient) Au−Au bonds on the inside. This is correctly predicted by the vibrational properties of these molecules in the form of the local stretching force constants, their associated BSO values, and the AI that measures the degree of σ-electron delocalization.

The results of this work can be a basis to predict the stability of larger gold clusters, which no longer might prefer a planar structure. Besides the Clar's rule for 3-rings, one must consider stabilization via peripheral electron delocalization and the avoidance of other highly destabilized subunits such as the tetracyclic and bicyclic Au_4 or the hexacyclic Au_6 unit. Work is in progress to provide a general rationale for the stability of larger gold clusters.

π-Aromaticity has been described as a multidimensional problem,[13] which means that by measuring different properties of an aromatic molecule different manifestations of aromaticity are obtained. The same holds for σ-aromaticity: (i) Energetic properties reveal the impact of aromaticity on the molecular stability. (ii) The electron density distribution and its Laplacian provide an insight into the spatial extension of aromaticity (one-, two-, or three-dimensional delocalization). (iii) Vibrational force constants reflect via BSO and AI the bond strength and the degree of electron delocalization. (iv) Magnetic properties such as the NICS values are the basis for a hypersensitive measure of magnetic anisotropy and potential orbital currents. Since the energy is a robust but very insensitive measure and the magnetic properties are too sensitive indicating even the weakest delocalization effects, the AI based on local stretching force constants seems to be the most useful measure, especially if it is combined with electron or energy density properties: In this way, a sensitive but not too sensitive measure of electron delocalization is obtained, by which one can distinguish local and global electron delocalization.

■ ASSOCIATED CONTENT

Supporting Information

The Supporting Information is available free of charge on the ACS Publications website at DOI: 10.1021/acs.inorgchem.7b00404.

Electron density paths and density critical points of the Au_m clusters; Cartesian coordinates; recalibration of the AI equation using 3c-2e Au_2Zn^{2+} as reference HOMO−LUMO orbital energy gaps (in eV), NICS(0), and NICS(1) values (in ppm) for the 3c-2e Li_3^+ and H_3^+ systems (PDF)

■ AUTHOR INFORMATION

Corresponding Authors

*E-mail: dieter.cremer@gmail.com. (D.C.)
*E-mail: majing@nju.edu.cn. (J.M.)

ORCID

Dieter Cremer: 0000-0002-6213-5555
Jing Ma: 0000-0001-5848-9775

Author Contributions

§These authors equally contributed.

Notes

The authors declare no competing financial interest.

■ ACKNOWLEDGMENTS

This work was supported by the National Natural Science Foundation of China (Grant Nos. 21290192 and 21673111) and the National Science Foundation of the USA (Grant No. CHE 1464906). We are grateful to the High Performance Computing Centers of Nanjing Univ. and SMU for providing sufficient computational resources. The authors acknowledge financial support by CAPES (Brazil; Fellowship Grant BEX 9534-13-0). One of the authors (C.L.) was also supported by the Program A for Outstanding Ph.D. Candidate of Nanjing Univ.

■ REFERENCES

(1) Haruta, M.; Kobayashi, T.; Sano, H.; Yamada, N. Novel gold catalysts for the oxidation of carbon monoxide at a temperature far below 0 °C. *Chem. Lett.* **1987**, *16*, 405−408.

(2) Schwerdtfeger, P. Gold goes nano - from small clusters to low-dimensional assemblies. *Angew. Chem., Int. Ed.* **2003**, *42*, 1892−1895.

(3) Daniel, M. C.; Astruc, D. Gold nanoparticles: assembly, supramolecular chemistry, quantum-size-related properties, and applications toward biology, catalysis, and nanotechnology. *Chem. Rev. (Washington, DC, U. S.)* **2004**, *104*, 293−346.

(4) Pyykkö, P. Structural properties: Magic nanoclusters of gold. *Nat. Nanotechnol.* **2007**, *2*, 273−274.

(5) Johnston, P.; Carthey, N.; Hutchings, G. J. Discovery, development, and commercialization of gold catalysts for acetylene hydrochlorination. *J. Am. Chem. Soc.* **2015**, *137*, 14548−14557.

(6) Guo, R.; Balasubramanian, K.; Wang, X.; Andrews, L. Infrared vibronic absorption spectrum and spin−orbit calculations of the upper spin−orbit component of the Au_3 ground state. *J. Chem. Phys.* **2002**, *117*, 1614−1620.

(7) Gruene, P.; Rayner, D. M.; Redlich, B.; van der Meer, A. F. G.; Lyon, J. T.; Meijer, G.; Fielicke, A. Structures of neutral Au_7, Au_{19}, and Au_{20} clusters in the gas phase. *Science* **2008**, *321*, 674−676.

(8) De, H. S.; Krishnamurty, S.; Mishra, D.; Pal, S. Finite temperature behavior of gas phase neutral ($3 \leq n \leq 10$) clusters: a first principles investigation. *J. Phys. Chem. C* **2011**, *115*, 17278−17285.

DOI: 10.1021/acs.inorgchem.7b00404
Inorg. Chem. 2017, 56, 5793−5803

(9) Zanti, G.; Peeters, D. Electronic structure analysis of small gold clusters Au_m ($m \leq 16$) by density functional theory. *Theor. Chem. Acc.* **2013**, *132*, 1300.
(10) Sergeeva, A. P.; Boldyrev, A. I. Rational design of small 3D gold clusters. *J. Cluster Sci.* **2011**, *22*, 321−329.
(11) Xu, W. W.; Zhu, B.; Zeng, X. C.; Gao, Y. A grand unified model for liganded gold clusters. *Nat. Commun.* **2016**, *7*, 13574.
(12) Gilb, S.; Weis, P.; Furche, F.; Ahlrichs, R.; Kappes, M. M. Structures of small gold cluster cations (Au_n^+, $n < 14$): Ion mobility measurements versus density functional calculations. *J. Chem. Phys.* **2002**, *116*, 4094−4101.
(13) Cremer, D. Pros and cons of σ-aromaticity. *Tetrahedron* **1988**, *44*, 7427−7454.
(14) Cremer, D.; Kraka, E.; Szabo, K. J. General and theoretical aspects of the cyclopropyl group. In *The Chemistry of Functional Groups: The Chemistry of the Cyclopropyl Group;* Rappoport, Z., Ed.; John Wiley: New York, NY, 1995; Vol. 2, p 43.
(15) Dewar, M. J. σ-Conjugation and σ-aromaticity. *Bull. Soc. Chim. Belg.* **1979**, *88*, 957−967.
(16) Cremer, D.; Gauss, J. Theoretical determination of molecular structure and conformation. 20. reevaluation of the strain energies of cyclopropane and cyclobutane—CC and CH bond energies, 1, 3 interactions, and σ-aromaticity. *J. Am. Chem. Soc.* **1986**, *108*, 7467−7477.
(17) Cremer, D.; Kraka, E. Theoretical determination of molecular structure and conformation. 15. three-membered rings: bent bonds, ring strain, and surface delocalization. *J. Am. Chem. Soc.* **1985**, *107*, 3800−3810.
(18) Cremer, D.; Kraka, E. Theoretical determination of molecular structure and conformation. 16. substituted cyclopropanes—an electron density model of substituent—ring interactions. *J. Am. Chem. Soc.* **1985**, *107*, 3811−3819.
(19) Wu, W.; Ma, B.; Schleyer, P. V. R.; Mo, Y.; et al. Is cyclopropane really the σ-aromatic paradigm? *Chem. - Eur. J.* **2009**, *15*, 9730−9736.
(20) Havenith, R. W.; De Proft, F.; Fowler, P. W.; Geerlings, P. σ-Aromaticity in: insights from ring-current maps. *Chem. Phys. Lett.* **2005**, *407*, 391−396.
(21) Ma, J.; Hozaki, A.; Inagaki, S. Pentagon stability: cyclic delocalization of lone pairs through σ conjugation and design of polycyclophosphanes. *Inorg. Chem.* **2002**, *41*, 1876−1882.
(22) Freitag, K.; Gemel, C.; Jerabek, P.; Oppel, I. M.; Seidel, R. W.; Frenking, G.; Banh, H.; Dilchert, K.; Fischer, R. A. The σ-aromatic clusters $[Zn_3]^+$ and $[Zn_2Cu]$: embryonic brass. *Angew. Chem., Int. Ed.* **2015**, *54*, 4370−4374.
(23) Díaz-Cervantes, E.; Poater, J.; Robles, J.; Swart, M.; Solà, M. Unraveling the origin of the relative stabilities of group 14 $M_2N_2^{2+}$ (M, N= C, Si, Ge, Sn, and Pb) isomer clusters. *J. Phys. Chem. A* **2013**, *117*, 10462−10469.
(24) Cheng, S. B.; Berkdemir, C.; Castleman, A. W. Observation of d−p hybridized aromaticity in lanthanum-doped boron clusters. *Phys. Chem. Chem. Phys.* **2014**, *16*, 533−539.
(25) Zhu, C.; Zhou, X.; Xing, H.; An, K.; Zhu, J.; Xia, H. σ-Aromaticity in an unsaturated ring: osmapentalene derivatives containing a metallacyclopropene unit. *Angew. Chem., Int. Ed.* **2015**, *54*, 3102−3106.
(26) Hao, Y.; Wu, J.; Zhu, J. σ Aromaticity dominates in the unsaturated three-membered ring of cyclopropametallapentalenes from groups 7- 9: A DFT study. *Chem. - Eur. J.* **2015**, *21*, 18805−18810.
(27) Tanaka, H.; Neukermans, S.; Janssens, E.; Silverans, R. E.; Lievens, P. σ Aromaticity of the bimetallic Au_5Zn^+ cluster. *J. Am. Chem. Soc.* **2003**, *125*, 2862−2863.
(28) Becke, A. D. Density-functional thermochemistry. III. The role of exact exchange. *J. Chem. Phys.* **1993**, *98*, 5648−5652.
(29) Lee, C.; Yang, W.; Parr, R. G. Development of the Colle-Salvetti correlation-energy formula into a functional of the electron density. *Phys. Rev. B: Condens. Matter Mater. Phys.* **1988**, *37*, 785.
(30) Hay, P. J.; Wadt, W. R. Ab initio effective core potentials for molecular calculations. Potentials for the transition metal atoms Sc to Hg. *J. Chem. Phys.* **1985**, *82*, 270−283.
(31) Wadt, W. R.; Hay, P. J. Ab initio effective core potentials for molecular calculations. Potentials for main group elements Na to Bi. *J. Chem. Phys.* **1985**, *82*, 284−298.
(32) Hay, P. J.; Wadt, W. R. Ab initio effective core potentials for molecular calculations. Potentials for K to Au including the outermost core orbitals. *J. Chem. Phys.* **1985**, *82*, 299−310.
(33) Yanai, T.; Tew, D. P.; Handy, N. C. A new hybrid exchange-correlation functional using the Coulomb-attenuating method (CAM-B3LYP). *Chem. Phys. Lett.* **2004**, *393*, 51−57.
(34) Zhao, Y.; Truhlar, D. G. The M06 suite of density functionals for main group thermochemistry, thermochemical kinetics, noncovalent interactions, excited states, and transition elements: two new functionals and systematic testing of four M06-class functionals and 12 other functionals. *Theor. Chem. Acc.* **2008**, *120*, 215−241.
(35) Vydrov, O. A.; Scuseria, G. E. Assessment of a long-range corrected hybrid functional. *J. Chem. Phys.* **2006**, *125*, 234109.
(36) Vydrov, O. A.; Heyd, J.; Krukau, A. V.; Scuseria, G. E. Importance of short-range versus long-range Hartree-Fock exchange for the performance of hybrid density functionals. *J. Chem. Phys.* **2006**, *125*, 074106.
(37) Vydrov, O. A.; Scuseria, G. E.; Perdew, J. P. Tests of functionals for systems with fractional electron number. *J. Chem. Phys.* **2007**, *126*, 154109.
(38) Chai, J. D.; Head-Gordon, M. Long-range corrected hybrid density functionals with damped atom−atom dispersion corrections. *Phys. Chem. Chem. Phys.* **2008**, *10*, 6615−6620.
(39) Raghavachari, K.; Trucks, G. W.; Pople, J. A.; Head-Gordon, M. A fifth-order perturbation comparison of electron correlation theories. *Chem. Phys. Lett.* **1989**, *157*, 479−483.
(40) Perdew, J. P.; Burke, K.; Ernzerhof, M. Generalized gradient approximation made simple. *Phys. Rev. Lett.* **1996**, *77*, 3865−3868.
(41) Grimme, S.; Antony, J.; Ehrlich, S.; Krieg, H. A consistent and accurate ab initio parametrization of density functional dispersion correction (DFT-D) for the 94 elements H-Pu. *J. Chem. Phys.* **2010**, *132*, 154104.
(42) Grimme, S.; Ehrlich, S.; Goerigk, L. Effect of the damping function in dispersion corrected density functional theory. *J. Comput. Chem.* **2011**, *32*, 1456−1465.
(43) Peterson, K.; Puzzarini, C. Systematically convergent basis sets for transition metals. II. Pseudopotential-based correlation consistent basis sets for the group 11 (Cu, Ag, Au) and 12 (Zn, Cd, Hg) elements. *Theor. Chem. Acc.* **2005**, *114*, 283−296.
(44) Balabanov, N. B.; Peterson, K. A. Systematically convergent basis sets for transition metals. I. All-electron correlation consistent basis sets for the 3d elements Sc-Zn. *J. Chem. Phys.* **2005**, *123*, 064107.
(45) London, F. Théorie quantique des courants interatomiq-ues dans les combinaisons aromatiques. *J. Phys. Radium* **1937**, *8*, 397−409.
(46) McWeeny, R. Perturbation theory for the Fock-Dirac density matrix. *Phys. Rev.* **1962**, *126*, 1028.
(47) Ditchfield, R. Self-consistent perturbation theory of diamagnetism: I. A gauge-invariant LCAO method for NMR chemical shifts. *Mol. Phys.* **1974**, *27*, 789−807.
(48) Wolinski, K.; Hinton, J. F.; Pulay, P. Efficient implementation of the gauge-independent atomic orbital method for NMR chemical shift calculations. *J. Am. Chem. Soc.* **1990**, *112*, 8251−8260.
(49) Cheeseman, J. R.; Trucks, G. W.; Keith, T. A.; Frisch, M. J. A comparison of models for calculating nuclear magnetic resonance shielding tensors. *J. Chem. Phys.* **1996**, *104*, 5497−5509.
(50) Chen, Z.; Wannere, C. S.; Corminboeuf, C.; Puchta, R.; Schleyer, P. v. R. Nucleus-independent chemical shifts (NICS) as an aromaticity criterion. *Chem. Rev. (Washington, DC, U. S.)* **2005**, *105*, 3842−3888.
(51) Santos, J.; Tiznado, W.; Contreras, R.; Fuentealba, P. Sigma-pi separation of the electron localization function and aromaticity. *J. Chem. Phys.* **2004**, *120*, 1670−1673.

DOI: 10.1021/acs.inorgchem.7b00404
Inorg. Chem. 2017, 56, 5793−5803

(52) Konkoli, Z.; Cremer, D. A new way of analyzing vibrational spectra. I. Derivation of adiabatic internal modes. *Int. J. Quantum Chem.* **1998**, *67*, 1−9.
(53) Zou, W.; Kalescky, R.; Kraka, E.; Cremer, D. Relating normal vibrational modes to local vibrational modes with the help of an adiabatic connection scheme. *J. Chem. Phys.* **2012**, *137*, 084114.
(54) Zou, W.; Cremer, D. Properties of local vibrational modes: the infrared intensity. *Theor. Chem. Acc.* **2014**, *133*, 1−15.
(55) Zou, W.; Cremer, D. C2 in a box: determining its Intrinsic bond strength for the X1Σg+ ground state. *Chem. - Eur. J.* **2016**, *22*, 4087−4099.
(56) Kraka, E.; Larsson, J. A.; Cremer, D. Generalization of the Badger rule based on the use of adiabatic vibrational modes. *Vibrational Modes in Computational IR Spectroscopy;* Wiley: New York, 2010, 105−149.
(57) Zou, W.; Filatov, M.; Cremer, D. An improved algorithm for the normalized elimination of the small-component method. *Theor. Chem. Acc.* **2011**, *130*, 633−644.
(58) Cremer, D.; Zou, W.; Filatov, M. Dirac-exact relativistic methods: the normalized elimination of the small component method. *WIREs Comput. Mol. Sci.* **2014**, *4*, 436−467.
(59) Mayer, I. Bond orders and valences from ab initio wave functions. *Int. J. Quantum Chem.* **1986**, *29*, 477−483.
(60) Mayer, I. Bond order and valence indices: A personal account. *J. Comput. Chem.* **2007**, *28*, 204−221.
(61) Weinhold, F.; Landis, C. R. *Valency and Bonding, A Natural Bond Orbital Donor−Acceptor Perspective;* Cambridge University Press: New York, 2005.
(62) Bader, R. F. W. *Atoms in Molecules: A Quantum Theory;* Oxford University Press: Oxford, England,1994.
(63) Kalescky, R.; Kraka, E.; Cremer, D. Description of aromaticity with the help of vibrational spectroscopy: anthracene and phenanthrene. *J. Phys. Chem. A* **2014**, *118*, 223−237.
(64) Setiawan, D.; Kraka, E.; Cremer, D. Quantitative assessment of aromaticity and antiaromaticity utilizing vibrational spectroscopy. *J. Org. Chem.* **2016**, *81*, 9669−9686.
(65) Cremer, D. New ways of analyzing chemical bonding. *Modell. Struct. Prop. Mol.* **1987**, 128−144.
(66) Zou, W.; Izotov, D.; Cremer, D. New way of describing static and dynamic deformations of the Jahn-Teller type in ring molecules. *J. Phys. Chem. A* **2011**, *115*, 8731−8742.
(67) Frisch, M. J.; Trucks, G. W.; Schlegel, H. B.; Scuseria, G. E.; Robb, M. A.; Cheeseman, J. R.; Scalmani, G.; Barone, V.; Mennucci, B.; Petersson, G. A.; Nakatsuji, H.; Caricato, M.; Li, X.; Hratchian, H. P.; Izmaylov, A. F.; Bloino, J.; Zheng, G.; Sonnenberg, J. L.; Hada, M.; Ehara, M.; Toyota, K.; Fukuda, R.; Hasegawa, J.; Ishida, M.; Nakajima, T.; Honda, Y.; Kitao, O.; Nakai, H.; Vreven, T.; Montgomery, J. A., Jr.; Peralta, J. E.; Ogliaro, F.; Bearpark, M.; Heyd, J. J.; Brothers, E.; Kudin, K. N.; Staroverov, V. N.; Kobayashi, R.; Normand, J.; Raghavachari, K.; Rendell, A.; Burant, J. C.; Iyengar, S. S.; Tomasi, J.; Cossi, M.; Rega, N.; Millam, J. M.; Klene, M.; Knox, J. E.; Cross, J. B.; Bakken, V.; Adamo, C.; Jaramillo, J.; Gomperts, R.; Stratmann, R. E.; Yazyev, O.; Austin, A. J.; Cammi, R.; Pomelli, C.; Ochterski, J. W.; Martin, R. L.; Morokuma, K.; Zakrzewski, V. G.; Voth, G. A.; Salvador, P.; Dannenberg, J. J.; Dapprich, S.; Daniels, A. D.; Farkas, Ö.; Foresman, J. B.; Ortiz, J. V.; Cioslowski, J.; Fox, D. J. *Gaussian09, Revision D.01;* Gaussian Inc.: Wallingford, CT, 2013.
(68) Werner, H.-J.; Knowles, P. J.; Knizia, G.; Manby, F. R.; Schütz, M. Molpro: a general-purpose quantum chemistry program package. *WIREs Comput. Mol. Sci.* **2012**, *2*, 242−253.
(69) Kraka, E.; Zou, W.; Filatov, M.; Gräfenstein, J.; Gauss, J.; He, Y.; Wu, A.; Konkoli, Z.; He, Z.; Cremer, D. *COLOGNE16;* Southern Methodist University: Dallas, TX, 2016.
(70) Lu, T.; Chen, F. Multiwfn: a multifunctional wavefunction analyzer. *J. Comput. Chem.* **2012**, *33*, 580−592.
(71) Kalescky, R.; Kraka, E.; Cremer, D. Identification of the strongest bonds in chemistry. *J. Phys. Chem. A* **2013**, *117*, 8981−8995.
(72) Bersuker, I. B. *The Jahn-Teller Effect;* Cambridge University Press: Cambridge, England, 2006.
(73) Clar, E.; Schoental, R. *Polycyclic Hydrocarbons;* Academic Press: London, England, 1964; Vols. *1* & 2.
(74) Wu, J.; Zhu, J. The Clar structure in inorganic BN analogues of polybenzenoid hydrocarbons: Does it exist or not? *ChemPhysChem* **2015**, *16*, 3806−3813.

DOI: 10.1021/acs.inorgchem.7b00404
Inorg. Chem. 2017, 56, 5793−5803